

# The Effect of the Earthquake Incidence Angle on Seismic Demand of Reinforced Concrete Structures

C. Cantagallo, G. Camata & E. Spacone  
University "G. D'Annunzio" of Chieti-Pescara, Italy



## SUMMARY

Because of the uncertainty of the location of the epicenter of the next earthquake, the ground motion records should be applied at any direction relative to the structure which needs to be analyzed. The structural demand produced by Non-Linear Time-History Analyses (NLTHA) varies in function of the incidence angle of the seismic input. This study evaluates the seismic directionality effects by subjecting four three-dimensional reinforced concrete structures to different scaled and un-scaled bi-directional ground motion records oriented along nine incidence angles, whose values are between 0 and 180 degrees, with an increment of 22.5 degrees. The NLTHA performed applying the ground motions along the principal axes underestimate the structural demand prediction, especially when plan-irregular structures are analyzed. The ground motion records generate the highest demand when applied in the most flexible structural direction and a high energy content of the records increases the structural demand corresponding to this direction.

*Keywords: Incidence Angle, Bi-directional Ground Motions, Non-Linear Time History Analysis*

## 1. INTRODUCTION

Current design codes prescribe that two orthogonal simultaneously acting seismic horizontal components have to be applied along the principal structural axes to compute the seismic action effects. The issue is mostly of interest for Non-Linear Time History Analyses (NLTHA). In some cases, for irregular structures, it may be difficult to define the principal structural axes. Furthermore previous studies (Rigato and Medina, 2007; Hosseini and Salemi, 2008) indicate that incidence directions different from the principal building directions may lead to unfavorable dynamic responses. Also, during an earthquake, the direction of the dominant excitation component (or the seismic input principal, uncorrelated direction, as defined by Penzien and Watabe, 1975) is not necessarily aligned with the principal structural axes. Thus, applying the main seismic component along a direction different from the principal structural axes may lead to higher demand on the structure. For this reason Eurocode 8 (UNI EN 1998-1:2005) states in §4.3.3.1(11)P: “*Whenever a spatial structural model is used, the design seismic action shall be applied along all relevant horizontal directions and their orthogonal horizontal axes. For buildings with resisting elements in two perpendicular directions these two directions shall be considered as the relevant directions*”. Since the relevant directions of an asymmetric complex structure are a priori unknown, several incidence angles should be considered in order to assess the maximum structural demand. The overall objective of this work is to investigate the importance of the ground motion incidence angle by analyzing the NLTHA of four asymmetric and symmetric structures subjected to two horizontal simultaneous un-correlated components of several ground motion inputs. Each ground motion record is applied with different incidence angles varying between 0 and 180 degrees with 22.5 degree increments.

## 2. GROUND MOTION RECORD SELECTION

The record selection used in this study is based on the Probabilistic Seismic Hazard Analysis (PSHA) derived from an Italian study carried out between 2004 and 2006 by the National Institute of Geophysics and Volcanology (INGV) and the Civil Protection Department (DPC). This work (<http://esse1.mi.ingv.it/>) provides the seismic hazard analysis and the disaggregation for each point of a regular grid made of approximately 16852 nodes covering the entire Italian territory.

Records are selected using an earthquake scenario with moment magnitude  $M_w$ , epicentral distance  $R$  and soil site class A. The  $M_w$ - $R$  bins are derived from seismic hazard disaggregation (Bazzurro and Cornell, 1999) which defines  $M_w$  and  $R$  providing the larger contribution to the seismic hazard at a specified probability of exceedance (Spallarossa and Barani, 2007). For the analyses presented in this study, a site located on rock soil in Sulmona (AQ-Italy) - 42.084° latitude and 13.962° longitude, was selected. 61 records (each consisting of two orthogonal components), with  $M_w$  between 5.5 and 6.5 and  $R$  between 15 and 30 km, were selected for a probability of exceedance of 10% in 50 years. Epicentral distances  $R$  smaller than 15 km were not considered in order to avoid “near-field” effects. The selected records were taken from two databases: the European Strong-Motion Database (ESD) and the Italian Accelerometric Archive (ITACA). In these databases the ground motion components (two horizontal and one vertical) are given with the orientation in which they were recorded. In general, these components are correlated because the recording instruments are not oriented along the principal directions of the ground motion (Penzien and Watabe, 1975). All selected records are then uncorrelated using a coordinate transformation formally identical to that used for stress transformations (Lopez et al., 2004).

Following a previous study by Cantagallo et al. (2012), the spectra corresponding to the un-scaled records are scaled to the spectral acceleration  $S_a(T^*)$  in which  $T^*$  is the “non-linear period”  $T^*$ . Cantagallo et al. (2012) show how  $S_a(T^*)$  permits to consider the elongation of the effective structural period during the non-linear analysis. This study also indicates that  $S_a(T^*)$  is well correlated with the deformation demand (expressed in Cantagallo et al. 2012 by the maximum interstory drift ratio) and it produces the lowest variability in structural demand among the input intensity measures investigated. The “non-linear period”  $T^*$  is obtained from non-linear static (pushover) analyses carried out in accordance with Eurocode 8 (UNI EN 1998-1:2005). Capacity curves representing the relation between base shear force and control node displacement are obtained from the MDOF systems and these curves are then transformed into those of an equivalent Single Degree of Freedom (SDOF) system and approximated by a bilinear elasto-perfectly plastic force–displacement curve.  $T^*$  is the period corresponding to the initial branch of the bilinear idealized curve and is computed from the following equation:

$$T^* = 2\pi \sqrt{\frac{m^* d_y^*}{F_y^*}} \quad (2.1)$$

where  $d_y^*$  and  $F_y^*$  are the yield displacement and the ultimate strength of the bilinear idealized system, respectively, and  $m^*$  is the mass of the equivalent SDOF system (Eurocode 8, UNI EN 1998-1:2005: Annex B). The  $T^*$  values vary depending on the distribution of lateral loads and the loading direction. However, in this study only the  $T^*$  values corresponding to a “uniform” pattern applied in the direction of the first linear period are used to obtain the scaling factors.

For each record and for any structural period  $T$ , a single spectral acceleration  $S_a(T)$  is obtained as the geometric mean of the two corresponding horizontal spectral components,  $S_{aX}(T)$  and  $S_{aY}(T)$ . As stated in Beyer and Bommer (2006), the geometric mean is the most widely used definition of the horizontal component of motion (Beyer and Bommer, 2006). A single spectrum is therefore computed from the spectral values of the X and Y components. More specifically, the spectral acceleration corresponding to the period  $T^*$  is defined as:

$$S_a(T^*) = \sqrt{S_{aX}(T^*) \cdot S_{aY}(T^*)} \quad (2.2)$$

Eqn. 2.2 consents to compute a single scale factor for both horizontal components of each record.

Given the pre-selection that produced 61 records, four accelerogram combinations were considered. Comb. 1 contains all 61, un-scaled, records. Strictly speaking, these 61 records are not spectrum-compatible according to Eurocode 8 (UNI EN 1998-1:2005). The other three combinations contain scaled records and are spectrum-compatible. Comb. 2 and Comb. 3 consist of 20 records (each with two orthogonal components), while Comb. 4 consists of 7 records only. Eurocode 8 (UNI EN 1998-1:2005) prescribes that if 7 or more records are used, the average value of the seven maximum demands obtained for each record can be used as design value.

### 3. REINFORCED CONCRETE STRUCTURES AND STRUCTURAL MODELS

Four reinforced concrete structures (referred to as Structure 1, Structure 2, Structure 6 and Structure 8) were selected according to their structural configuration. For consistency with previous and ongoing work, the building labeling follows the numbering already used in Cantagallo et al. (2012). The structures were selected in order of increasing plan and elevation irregularity and are shown in Fig. 3.1. The structural models and the NLTHA were carried out with the commercial computer software Midas Gen 7.21 (Midas, 2007) using a force-based fiber-section beam model (Spacone et al., 1996) for the columns (with four Gauss-Lobatto integration points) and linear elastic elements for all beams. Floor diaphragms were used. Concrete was modeled with the Kent and Park (1971) constitutive law with  $f_{ck} = 20 \text{ MPa}$ , strain at maximum compressive strength  $\varepsilon_{c0} = 0.003$  and ultimate strain  $\varepsilon_{cu} = 0.0165$ . The Menegotto and Pinto (1973) constitutive law was used for the reinforcing steel, with  $f_{yk} = 215 \text{ MPa}$  (Structure 6 and 8) and  $430 \text{ MPa}$  (Structure 1 and 2),  $E = 200 \text{ GPa}$  and strain hardening ratio  $b = 0.02$ . All structures were subjected to permanent gravity loads  $G_k = 3 \text{ kN/m}^2$  and live load  $Q_k = 2 \text{ kN/m}^2$ , both applied with a two-way distribution. The gravity loads were applied statically before dynamically applying the ground motion records at the structures' bases.



**Figure 3.1.** Structural configuration of Structures 1, 2, 6 and 8 (from left to right)

Structure 1 is a doubly symmetric 1-storey 1-bay frame. The structural configuration is regular, both in terms of mass and stiffness distributions. The beam span is  $5 \text{ m}$  and the column height is  $3 \text{ m}$ : beam and column cross sections are all  $30 \times 30 \text{ cm}$ . The columns are reinforced with four  $12 \text{ mm}$  diameter rebars and their sections are subdivided into  $10 \times 10$  fibers.

Structure 2 is a 1-storey rectangular multi-bay structure. It can be generally defined as regular, but because of the column geometry, the structure has a longitudinal stiffness that is much higher than the transversal one. The plan dimensions are  $15 \times 3 \text{ m}$ . The beam and column cross sections are  $30 \times 60 \text{ cm}$ . The columns are reinforced with four  $14 \text{ mm}$  diameter rebars and their sections are subdivided into  $6 \times 12$  concrete fibers.

Structure 6 is a 2-storey rectangular multi-bay structure  $15 \times 3 \text{ m}$  in plan and  $6 \text{ m}$  high. In addition, a  $6 \text{ m}$  high,  $0.2 \text{ m}$  thick reinforced concrete wall is placed eccentrically. The three transverse frames are not equally spaced as the middle frame is placed  $2.5 \text{ m}$  away from the geometric center. The structure is regular in elevation, but plan-irregular because of the high eccentricity between mass and stiffness

centers in the longitudinal direction. The column sections are 20x40 cm and are reinforced with four 10 mm diameter rebars. The column sections are subdivided in 4x8 concrete fibers. The shear wall is modeled with elastic wall elements.

Structure 8 is a 3-storey multi-bay structure with an L-shaped plan configuration. A concrete wall ( $L = 3\text{ m}$ ,  $H = 9\text{ m}$ ,  $t = 0.2\text{ m}$ ) is included in the transverse frame and is modeled with elastic wall elements. The distributions of the structural elements and loads give the structure a significant irregularity both in plan and in elevation. The structure is 15x6 m in plan. Beams and columns are identical to those of Structure 6.

In order to investigate the effects of the ground motion direction variability on the structural demand, a single Engineering Demand Parameter (EDP), the Maximum Interstory Drift Ratio MIDR, was considered (Faggella et al., 2012). MIDR is computed as the maximum percentage interstory drift DXY over time (the record duration), that is  $\text{MIDR} = \max|\text{DXY}(t)|$ . For each record, the interstory drift ratio at an instant  $t$  is computed as:

$$\text{DXY}(t) = \sqrt{\text{DX}(t)^2 + \text{DY}(t)^2} \quad (3.1)$$

where  $\text{DX}(t)$  and  $\text{DY}(t)$  are the instantaneous interstory drifts in the X and Y directions, respectively, between the centers of mass of two adjacent floors.

#### 4. RESULTS WITH UN-SCALED GOUND MOTION RECORDS

The results of the MIDR obtained by analyzing the four selected structures of Fig. 3.1 by NLTHA using all recorded 61 pairs of un-scaled accelerograms are summarized in the polar graphs of Fig. 4.1. For Structure 1 the variation of the EDP MIDR is similar for all incidence angles, while for the other structures they vary significantly, depending on the incidence angles. For example, the maximum MIDR( $\theta$ ), that is the maximum MIDR over all incidence angles  $\theta$ , is found, for Structure 6, for an incidence angle  $\theta = 22.5^\circ$  and it is equal to  $\text{MIDR}(22.5^\circ) = 2.37\%$ .

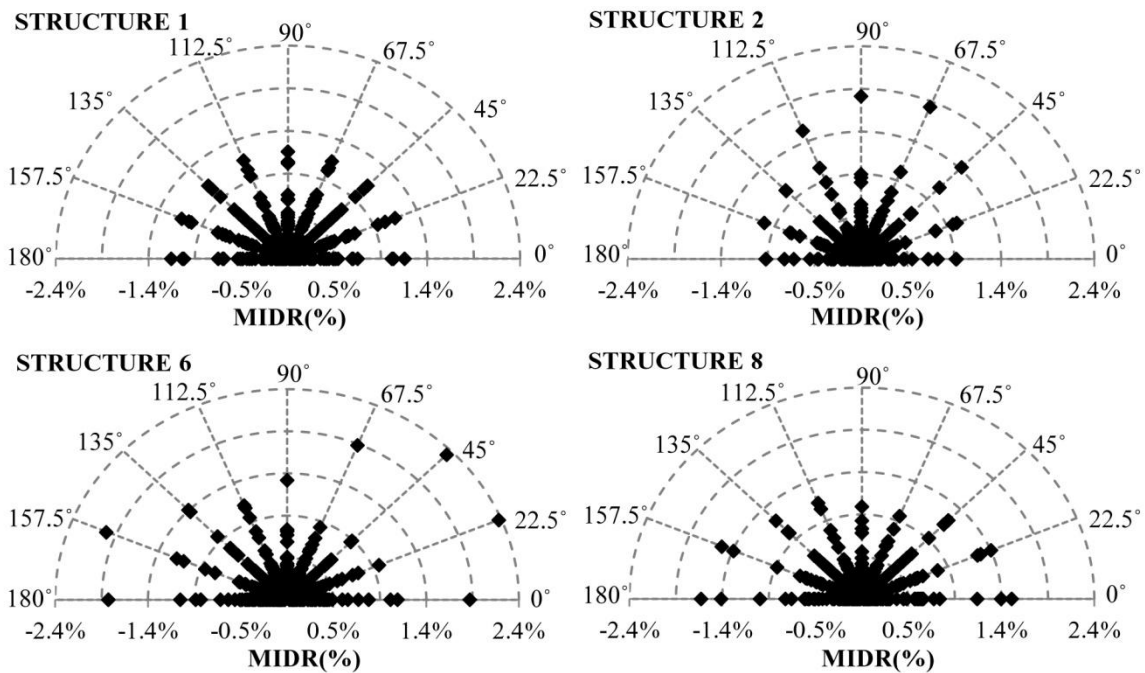


**Figure 4.1.** MIDR of Structures 1, 2, 6 and 8 as a function of the incidence angle of the seismic input for the selected set of 61 pairs of un-scaled accelerograms

The results of Fig. 4.1 may be better interpreted if they are normalized. Athanatopoulou A. M. (2005) proposes using the orientation effect ratio,  $r(\theta_i)$ , defined as:

$$r(\theta_i) = \frac{\max |R_{,p}(\theta_i, t)|}{\max |R_{,x}(t)|} \quad (4.1)$$

where

- $\theta$  is the orientation of the two horizontal excitation axes with respect to the structure reference axes; the translational components of ground motions are oriented according to the angles  $\theta$  and  $\theta + 90$  degrees;
- $\max |R_{,p}(\theta_i, t)|$  is the absolute value of the MIDR for an incident angle  $\theta = \theta_i$ ;
- $\max |R_{,x}(t)|$  is the absolute value of the MIDR when the input records are aligned with the structural reference axes (i.e.  $\theta = 0$ ).

Fig. 4.2 shows the orientation effect ratio  $r(\theta_i)$  for the data already shown in Fig. 4.1. Directionality effects obtained from Structure 2 are much larger than those obtained from the other structures. For this particular structure the maximum  $r(\theta_i)$  is 9.14 and it is obtained with record 006331 (database ESD,  $M_w = 6.4$ ;  $R = 22$  km) for an incident angle  $\theta = 67.5^\circ$ . The average  $r(\theta_i)$  corresponding to the same incidence angle is equal to 1.95.

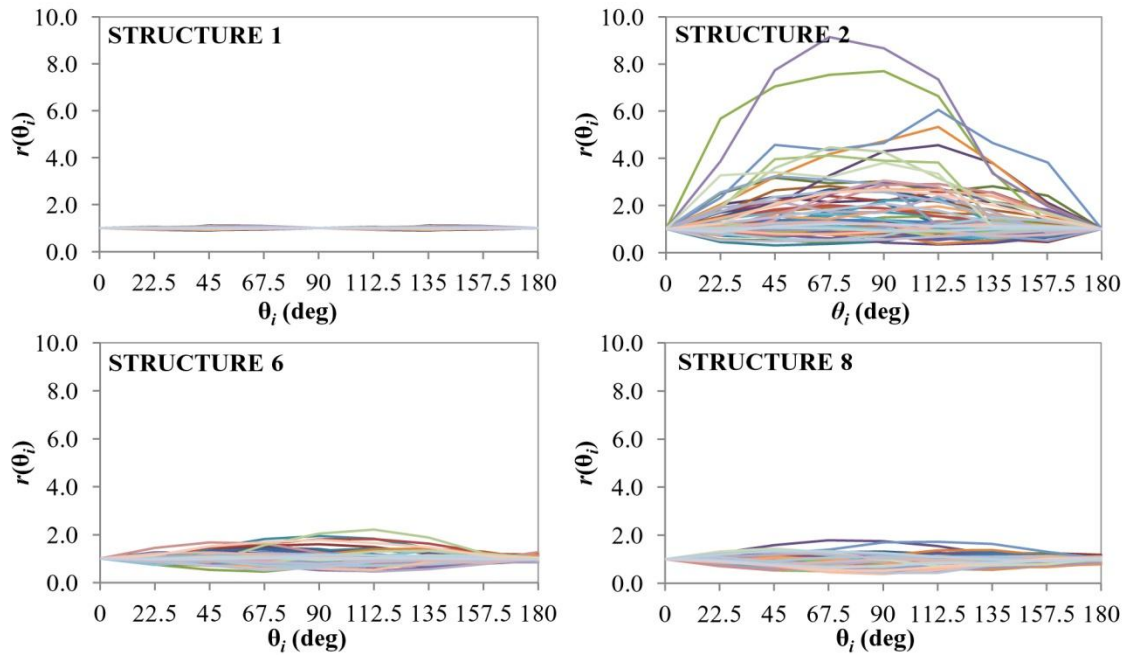


**Figure 4.2.** Variation of  $r(\theta_i)$  for Structures 1, 2, 6 and 8 for the 61 un-scaled records selected according to the M-R target scenario

The influence of the incidence angle on the seismic demand varies depending on both structural configuration and specific characteristics of each examined record. The influence of the structural configuration is investigated in more detail by analyzing the variation of structural demand on Structure 2 for a single record (000055 from database ESD,  $M_w = 6.3$ ;  $R = 23$  km) over time. Fig. 4.3 shows the evolution of  $DX(t)$  and  $DY(t)$  for the given ground motion. The nine different plots refer to nine different incidence angles. The lack of intermediate bays makes Structure 2 particularly flexible in the Y direction, generating a significant difference between the stiffness and strength in its two principal directions. The uncorrelation process (Penzien and Watabe, 1975) leads to a first principal component characterized by a larger acceleration intensity than the second principal component. This explains why the DYs are largest when  $\theta = 90^\circ$ , which is when the ground motion principal

component is aligned with the more flexible principal direction of the structure.

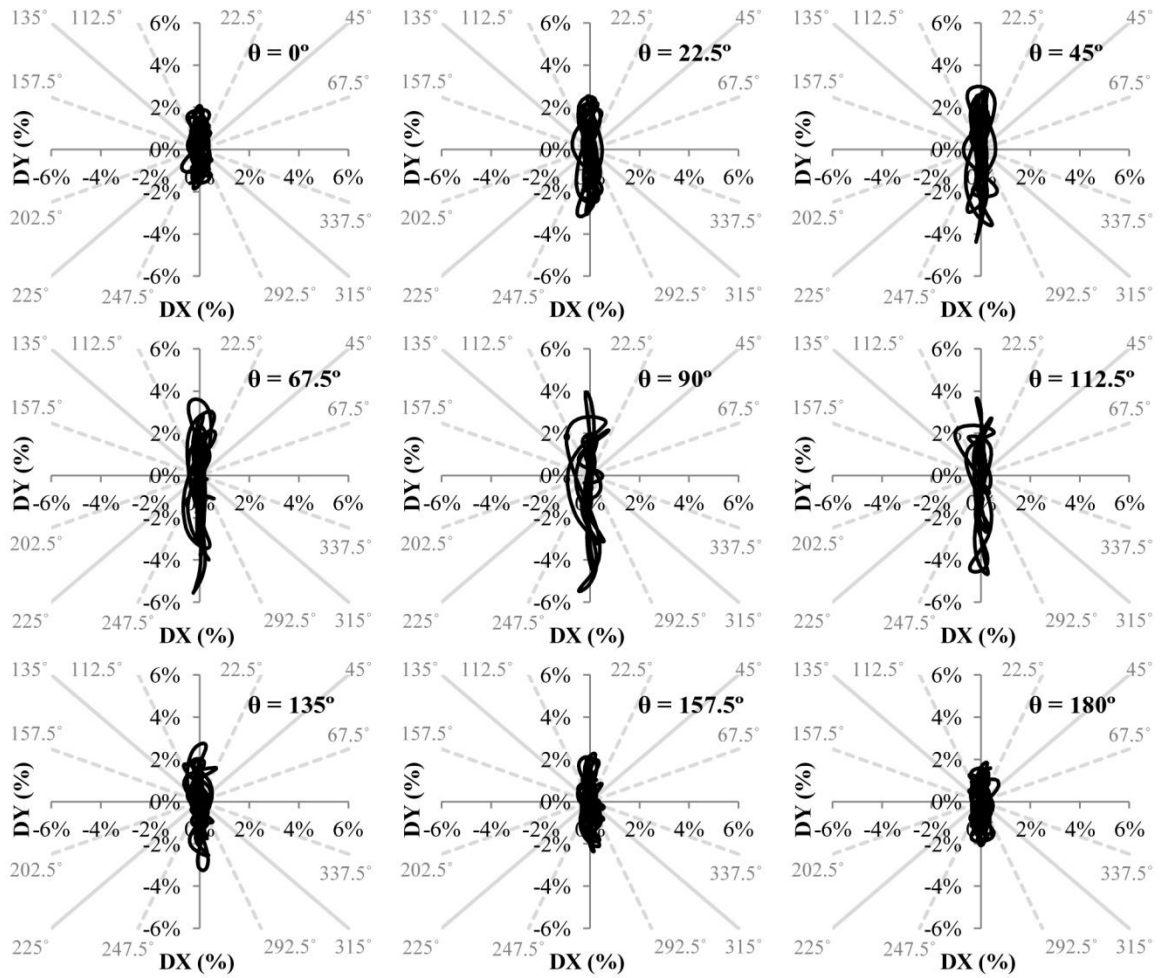


**Figure 4.3.** Variation of  $r(\theta_i)$  for Structures 1, 2, 6 and 8 for the 61 un-scaled records selected according to the M-R target scenario

To explain the influence of the characteristics of each examined record on the seismic demand variation with the incidence angle, the energy content of the 61 selected records is analyzed. The energy content of a single ground motion horizontal  $i$ -component (with  $i = X, Y$ ) is evaluated through the Specific Energy Density SED defined as:

$$SED_i = \int_0^{t_1} [v_i(t)]^2 dt \quad (4.2)$$

where  $v(t)$  is the ground motion velocity and  $t_1$  is the ground motion duration. The SED for the single recorded ground motion is computed as the geometric mean of the SEDs of the two principal components  $SED_X$  and  $SED_Y$ .

Fig. 4.4 shows the correlations between the SED values corresponding to each un-scaled record and MIDR( $\theta$ ) obtained by subjecting Structure 2 to different incident angles. The measure of the correlation between the two parameters is estimated through the determination coefficients  $R^2$ . These coefficients, whose values range between 0 and 1, reveal how closely the predicted value ( $Y_{pi}$ ) through a trendline corresponds to the actual data ( $Y_i$ ):

$$R^2 = \frac{\sum_i^n (Y_{pi} - Y_m)^2}{\sum_i^n (Y_i - Y_m)^2} \quad (4.3)$$

where  $Y_m$  = mean value and  $n$  = total number of points.

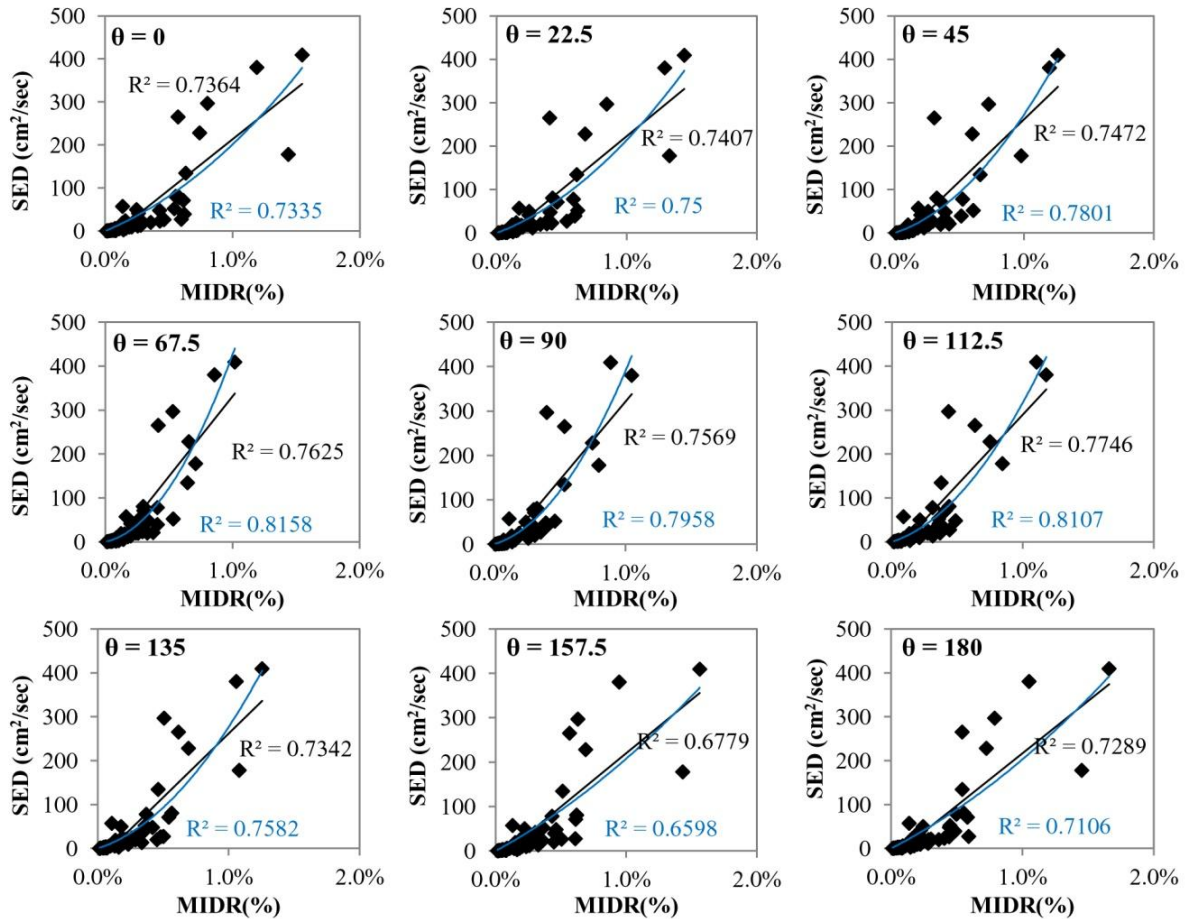


**Figure 4.4.** Correlations between the MIDRs obtained subjecting Structure 8 to the 61 records selected at ULS oriented along nine different incident angles and the corresponding SED values.

The  $R^2$  coefficients are based on linear and polynomial regression lines fitted through the data. The forms of the linear and polynomial relationships are respectively  $y = ax+c$  and  $y = ax+bx^2$ , where  $a$ ,  $b$  and  $c$  are constant coefficients. Table 4.1 shows the  $R^2$  values obtained by correlating the SED and MIDR values for all analyzed structures and incidence angles. The energy content of the un-scaled records have a good correlation with the seismic demand of Structure 6 and Structure 8. Since these structures have a high non-linear behaviour, the effects of inelasticity and ground motion duration are implicitly captured by the energy-based ground motion parameters (Mollaioli et al. 2011), as they are directly related to the number of cycles of the oscillator response.

**Table 4.1.** Coefficients of determination  $R^2$  obtained from correlations between SED values and MIDR's calculated from the four structures subjected to the 61 un-scaled records selected at the ULS.

Coefficients of Determination $R^2$									
Linear Regression Line					Polynomial Regression Line				
$\theta_i$	Str. 1	Str. 2	Str.6	Str. 8	$\theta_i$	Str. 1	Str. 2	Str.6	Str. 8
0°	0.4555	0.3979	0.6893	0.7364	0°	0.5140	0.4027	0.6783	0.7335
22.5°	0.4401	0.4407	0.6738	0.7407	22.5°	0.4902	0.463	0.6567	0.7500
45°	0.4310	0.4788	0.6753	0.7472	45°	0.4871	0.4948	0.6588	0.7801

67.5°	0.4421	0.5301	0.7508	0.7625	67.5°	0.5047	0.5372	0.7090	0.8158
90°	0.4555	0.5444	0.7891	0.7569	90°	0.5140	0.5588	0.7861	0.7958
112.5°	0.4401	0.5940	0.7310	0.7746	112.5°	0.4902	0.6304	0.7684	0.8107
135°	0.4310	0.5423	0.7154	0.7342	135°	0.4871	0.6039	0.7082	0.7582
157.5°	0.4421	0.4865	0.7129	0.6779	157.5°	0.5047	0.5218	0.6986	0.6598
180°	0.4555	0.3979	0.7067	0.7289	180°	0.514	0.4027	0.6895	0.7106

## 5. RESULTS WITH SCALED GROUND MOTION RECORDS

Fig. 5.1 shows the variation of the orientation effect ratios  $r(\theta_i)$  obtained by subjecting the four analyzed structures to the three combinations of scaled records with nine different incidence angles. The directionality effects are larger for the irregular structures (Structures 2, 6, and 8), especially when they are subjected to several specific records. For example, Comb. 2 applied on Structure 6 along  $\theta = 112.5^\circ$  produces a maximum  $r(\theta_i)$  equal to 4.83. The average  $r(\theta_i)$  corresponding to the same structure, combination and incidence angle is 1.22.

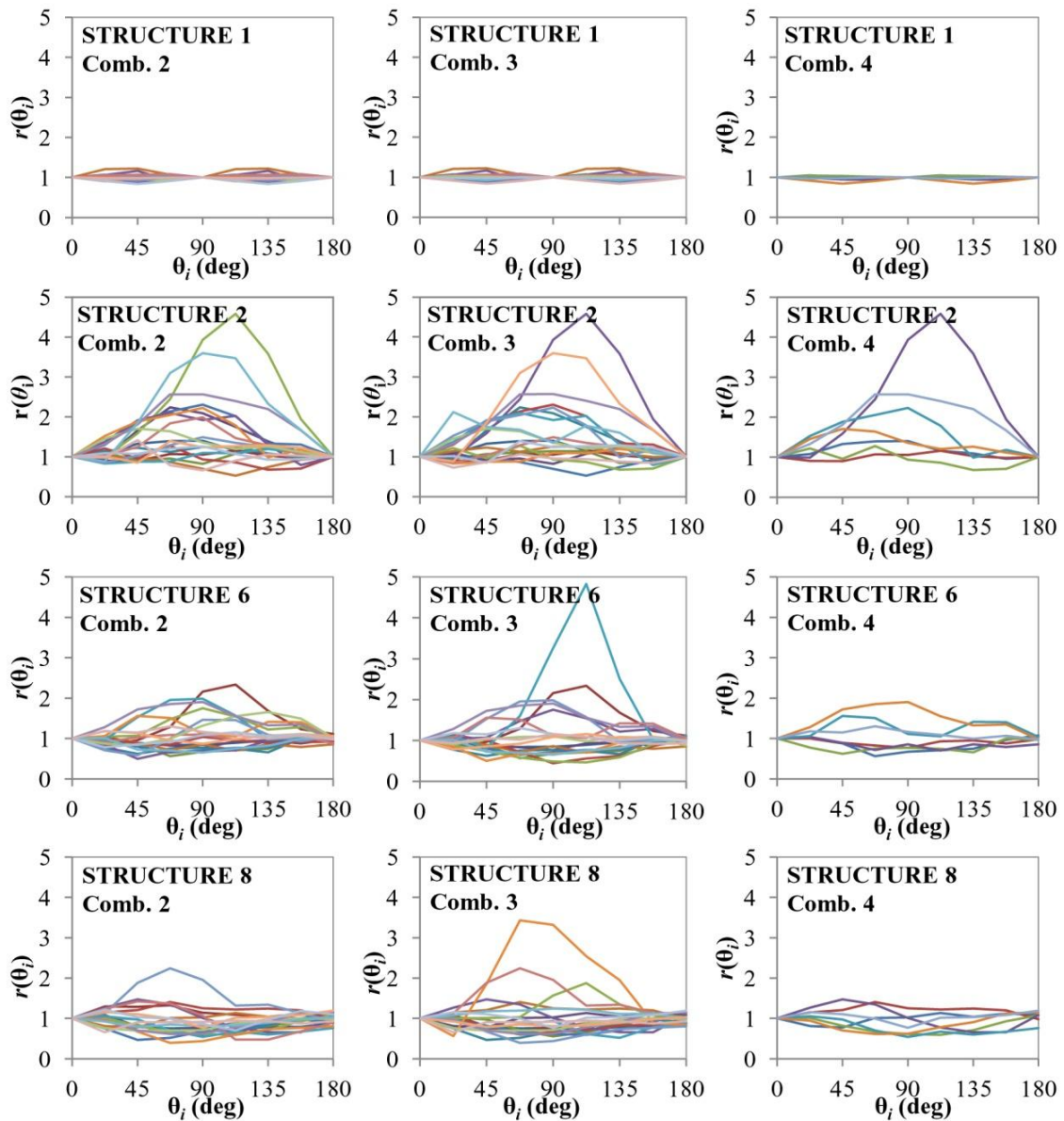


**Figure 5.1.**  $r(\theta_i)$  variation of MIDR on Structures 1, 2, 6 and 8 for each of the three combinations of spectrum-compatible records considered for each structure

The analysis of the  $r(\theta_i)$  values also indicates that the orientation effects generated from the spectrum-compatible combinations are lower than those computed for the un-scaled accelerograms, for which the maximum  $r(\theta_i)$ , obtained from Structure 2 at  $\theta = 67.5^\circ$ , is equal to 9.14 and the average  $r(\theta_i)$  corresponding to the same incidence angle is 1.93.

## 5. SUMMARY AND CONCLUSIONS

This paper analyzes the critical responses of four regular and irregular structures subjected to several ground motion records applied at different incidence angles, ranging between 0 and 180 degrees, with 22.5 degree increments. The structures are analyzed using Non-Linear Time History Analyses. The ground motion inputs consist of both scaled and un-scaled records with two horizontal un-correlated components. The un-scaled records consist of 61 pairs of accelerograms selected for a 10% in 50 years probability of exceedance scenario, while the scaled ground motions consist of three combinations of spectrum-compatible records, two with 20 and one with 7 pairs of accelerograms, scaled to the non-linear spectral acceleration  $S_a(T^*)$ . The principal results presented in this paper can be summarized as follows:

1. The structural demand on a doubly-symmetric 1-storey reinforced concrete structure does not vary significantly as a function of the incidence angle. Conversely, MIDRs for plan-irregular reinforced concrete structures vary considerably depending on the incidence angle. More specifically, the maximum orientation effect ratios  $r(\theta_i)$  obtained from the un-scaled ground motions show significant differences between the EDP computed by applying the seismic input along different incidence angles. This behavior is due to the fact that plan-irregular buildings tend to have significantly different stiffness and capacity in different directions. The applied ground motion generates the highest demand when applied in the most flexible direction.
2. Correlations between the energy content, measured by the Specific Energy Density SED, of the 61 un-scaled records and the MIDRs obtained by applying the ground motions at different incidence angles, show that the demand on the plan-irregular structures is well correlated with the ground motion SEDs. High energy content records tend to produce high MIDR( $\theta$ ) when they are applied along the more flexible structural direction. For regular structures this trend is not as visible because their behaviour, in terms of flexibility and strength, does not vary significantly along different directions.
3. The NLTHAs carried out with the sets of spectrum-compatible scaled accelerograms confirm that ground motion records applied on irregular structures produce very different EDPs depending on their incidence angle. The higher values of MIDR( $\theta$ ) and  $r(\theta_i)$  are both obtained when the ground motions are applied on the most irregular structures. The  $r(\theta_i)$  values show that the directionality effects generated by the scaled spectrum-compatible records are in general lower than those obtained for the un-scaled records.
4. The results of this study apply more specifically to existing buildings, which often present plan (and height) irregularities, with stiffness and strength that may vary significantly according to the loading direction considered. In these cases, the NLTHAs performed by applying the ground motion records along the principal axes may substantially underestimate the structural demand prediction. Since it is not possible to know *a priori* the incidence direction that will generate the highest demand, it is necessary to perform the NLTHAs for different incidence angles.

## ACKNOWLEDGEMENT

The authors would like to acknowledge the financial support from the ReLUIIS program of the Italian Civil Protection Agency (DPC), task 1.1.2, contract n. 823, 24/09/2009.

## REFERENCES

- Athanatopoulou, A.M. (2005). Critical orientation of three seismic components. *Engineering Structures* **27**, 301–312.
- Bazzurro, P., and Cornell, C.A. (1999). Disaggregation of seismic hazard. *Bulletin of the Seismological Society of America* **89:2**, 501-520.
- Beyer, K. and Bommer, J.J. (2006). Relationships between median values and between aleatory variabilities for different definitions of the horizontal component of motion. *Bulletin of the Seismological Society of America*, **96:4A**, 1512–1522.
- Bommer, J.J., and Acevedo, A.B. (2004). The use of real earthquake accelerograms as input to dynamic analysis, *Journal of Earthquake Engineering*, **8**, 43–91.
- Cantagallo, C., Camata, G., Spacone, E. and Corotis, R. (2012). The Variability of Deformation Demand with Ground Motion Intensity. *Probabilistic Engineering Mechanics*, **28**, 59-65.
- European Strong-motion Database (ESD). <http://www.isesd.cv.ic.ac.uk/ESD/frameset.htm>.
- Faggella, M., Barbosa, A.R., Conte, J.P., Spacone, E and Restrepo, J.I. (2012). Probabilistic Seismic Response Analysis of a 3-D Reinforced Concrete Building. *ASCE Journal of Structural Engineering*, submitted.
- Hosseini, M., Salemi, A. (2008). Studying the effect of earthquake excitation on the internal forces of steel building's elements by using nonlinear time history analyses. *14th World Conference on Earthquake Engineering*, Beijing, China, October 12-17.
- Italian ACcelerometric Archive (ITACA). <http://itaca.mi.ingv.it/ItacaNet/>.
- Kent, D.C., Park, R. (1971). Flexural members with confined concrete. *Journal of the Structural Division* **97:7**, 1969–1990.
- López, A., Hernández J.J. (2004). Structural Design for Multicomponent Seismic Motion. Vancouver, B.C., Canada, in *Proceedings, 13th World Conference on Earthquake Engineering*, paper 2171.
- Menegotto, M., Pinto, P.E. (1973). Method of analysis for cyclically loaded reinforced concrete plane frames including changes in geometry and nonelastic behavior of elements under combined normal force and bending. Zurich, in *Proceedings, IABSE Symposium on Resistance and Ultimate Deformability of Structures Acted on by Well Defined Repeated Loads*, pp. 112-123.
- Mollaioli, F., Bruno, S., Decanini, L., Saragoni, R. (2004). On the correlation between energy and displacement. Vancouver, B.C., Canada, in *Proceedings, 13th World Conference on Earthquake Engineering*, vol. CD, paper 161.
- MIDAS/Gen, ver. 7.21 (2007). [http://www.cspfea.net/midas\\_gen.php](http://www.cspfea.net/midas_gen.php).
- Penzien, J., and Watabe, M. (1975). Characteristics of 3-dimensional earthquake ground motion. *Earthquake Engineering and Structural Dynamics* **3:4**, 365-374.
- Rigato, A.B. and Medina, R.A. (2007). Influence of angle of incidence on seismic demands for inelastic single-storey structures subjected to bi-directional ground motions. *Engineering Structures*, **29:10**, pp. 2593-2601.
- Spacone, E., Filippou, F.C. Taucer, F. (1996). Fiber Beam-Column Model for Nonlinear Analysis of R/C Frames: I. Formulation. *Earthquake Engineering and Structural Dynamics* **25:7**, 711-725.
- Spallarossa, D., and Barani, S. (2007). Progetto DPC-INGV S1, Deliverable D14. <http://esse1.mi.ingv.it/d14.html>.
- UNI EN 1998-1:2005. *Eurocode 8: Design of structures for earthquake resistance - Part 1: General rules, seismic actions and rules for buildings*. EN1998-1-1, Brussels, 2004.